applied sciences

MDPI

*Review*

# Spinel Magnetic Iron Oxide Nanoparticles: Properties, Synthesis and Washing Methods

**Thomas Girardet [1], Pierre Venturini [1], Hervé Martinez [2], Jean-Charles Dupin [2], Franck Cleymand [1] and Solenne Fleutot [1,*]**

[1] Institut Jean Lamour, CNRS, Université de Lorraine, F-54000 Nancy, France
[2] Institut des Sciences Analytiques et de Physicochimie pour l'Environnement et les Matériaux—UMR 5254, CNRS/University of Pau and Pays de l'Adour/E2S UPPA, F-64000 Pau, France
* Correspondence: solenne.fleutot@univ-lorraine.fr

**Abstract:** Nanoparticles have experienced increasing interest over the past three decades owing to the development of new synthesis methods and the adaptation of analysis tools with spatial resolutions below one micrometer. Among the different types of nanoparticles developed in recent years (metals, metal oxides, silica, polymers, etc.), significant scientific interest has developed around iron oxide nanoparticles. This review will focus on these magnetic iron oxide nanoparticles. We will first discuss the magnetic properties of iron oxide nanoparticles, then the different methods of synthesis and washing. Finally, we will discuss some functionalization strategies of iron oxide nanoparticles which are developed within our research team.

**Keywords:** iron oxide nanoparticles; synthesis; characterization; magnetic properties; functionalization



**Citation:** Girardet, T.; Venturini, P.; Martinez, H.; Dupin, J.-C.; Cleymand, F.; Fleutot, S. Spinel Magnetic Iron Oxide Nanoparticles: Properties, Synthesis and Washing Methods. *Appl. Sci.* **2022**, *12*, 8127. https://doi.org/10.3390/app12168127

Academic Editor: Yurii K. Gun'ko

Received: 15 July 2022
Accepted: 11 August 2022
Published: 13 August 2022



## 1. Introduction

Nanomaterials and particularly nanoparticles NPs have experienced growing interest over the last three decades owing to the development of new synthesis methods and the adaptation of analysis tools with spatial resolutions below the micrometer.

The decrease at the nanoscale intrinsically leads to the increase in the surface to volume ratio which then exalts the behavior of the external atoms and the surface effects. The dimensional characteristic associated with the surface chemical state and the composition of nanoparticles leads to magnetic, optical, catalytic, and biological properties different from those of bulk materials, thus opening the way to many potential applications.

Among the different types of nanoparticles developed in recent years (metals, metal oxides, silica, polymers, etc.), significant scientific interest has developed around superparamagnetic iron oxide nanoparticles with a spinel structure. Indeed, the magnetic properties of these nanoparticles make them prime candidates for many applications [1], including biomedical ones such as contrast agent for magnetic resonance imaging or hyperthermia and treatment of cancers [1,2]. In this domain, for example, generally below a size of about 20 nm, these superparamagnetic nanoparticles will only be magnetized under the effect of an external magnetic field. Moreover, the absence of attractive magnetic forces between the NPs will promote their stability in suspension by limiting their tendency to agglomeration and aggregation. However, surface functionalization of iron oxide nanoparticles may be necessary to improve the dispersion and stability of suspended nanoparticles.

In this review, the crystal structures and magnetic properties of spinel-structured iron oxide nanoparticles will be presented. Then, the main methods of synthesis and washing of these nanoparticles will be discussed. Finally, the stabilization of iron oxide nanoparticles in solution will be discussed considering the experience of our team in the synthesis of iron oxide nanoparticles.

## 2. Crystal Structure and Magnetic Properties of Spinel Iron Oxide

In natural condition, iron oxide crystallizes according to four distinct structures:

- Hematite $\alpha$-$Fe_2O_3$ which crystallizes in a trigonal structure and in a space group $R\bar{3}ch$. In this compound, iron is at the oxidation state +III.
- Wustite $Fe_{1-x}O$ which presents a cubic structure according to the space group $Fm\bar{3}m$. This compound is most uncommon and is found almost exclusively in reducing environments. In this one, iron is mainly at the oxidation state +III.
- Magnetite $Fe_3O_4$ which crystallizes in a cubic structure according to the space group $Fd\bar{3}m$. In this crystallographic structure, called spinel, iron is presented at the oxidation state +II and +III.
- Maghemite $\gamma$-$Fe_2O_3$ which presents a cubic structure ($Fd\bar{3}m$ or $P4_132$) or a tetragonal structure ($P4_12_12$). The structure of this compound is related to the spinel structure, iron is only presented at the oxidation state +III. Maghemite is obtained by sweet oxidation of magnetite.

In this review, we will focus on magnetite and maghemite for their magnetic properties.

### *2.1. Crystal Structures*

#### 2.1.1. Magnetite Crystal Structure

The $Fe_3O_4$ magnetite crystallizes in a spinel type structure according to the space group $Fd\bar{3}m$ and presents a lattice parameter close to 0.8396 nm at room temperature (JCPDS card 04-015-8200).

The spinel structure was described for the first time by W.H. Bragg and S. Nishikawa in 1915 [3] and owes its name to the mineral $MgAl_2O_4$. Spinels present the general chemical formula $AB_{2\times4}$ with A and B as the metal cations $Fe^{2+}$ and $Fe^{3+}$ and X anions $O^{2-}$ for the magnetite.

Several types of spinel structures can be described according to the distribution of cations A and B in the interstitial sites: "direct", "reverse" spinel structure or an intermediate structure. Magnetite adopts a spinel structure called "reverse". Considering magnetite, the crystal lattice is constituted of 32 anions $O^{2-}$ forming a face-centered cubic network. One-eighth of the 64 tetrahedral sites (denoted A) generated by this anionic arrangement are occupied by the trivalent cations $Fe^{3+}$ and half of the 32 octahedral sites (denoted B) are occupied by divalent cations $Fe^{2+}$ and trivalent cations $Fe^{3+}$ (Figure 1). The magnetite formula can be written in the form $(Fe^{3+})^{tetra}[Fe^{2+}Fe^{3+}]^{octa}(O^{2-})_4$ to better represent the position of the ions $Fe^{2+}$ and $Fe^{3+}$ in the different sites of the structure.

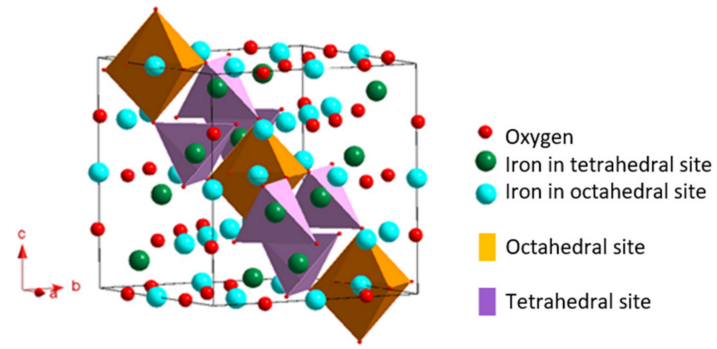


**Figure 1.** Representation of mesh of the crystallographic structure of magnetite. The octahedra and tetrahedra materialize on of the planes (111) of the mesh.

The magnetite can be partially oxidized. It will be named "sub stoichiometric magnetite" with chemical formula $Fe_{3-\delta}O_4$ where $\delta$ represents the deviation from stoichiometric of the magnetite. Totally oxidized magnetite is called maghemite.

2.1.2. Maghemite Crystal Structure

Maghemite, $\gamma$-$Fe_2O_3$, is obtained by the complete oxidation of magnetite. Divalent cations $Fe^{2+}$ are replaced by trivalent cations $F^{3+}$ and the electronic neutrality is assured by the apparition of cationic gaps.

Three distributions of cationic gaps have been identified for this compound [1] depending on the synthesis conditions (Figure 2):

- A random distribution of gaps in the octahedral sites of the mesh without deformation (in yellow on the Figure 2A) with the same probability of presence of the gap and an occupation rate of 5/6. In this case, the crystallographic structure of maghemite stays cubic and describes the space group $Fd\bar{3}m$. Its lattice parameter of 0.8354 nm at room temperature (JCPDS card 04-013-7114) is slightly reduced ($\Delta = -0.0039$ nm) compared to that of magnetite. This reduction translates the slight contraction of the structure due to the appearance of gaps.
- A partially organized division of gaps in the defined octahedral sites of the mesh (in yellow on the Figure 2B) always without deformation with an occupation rate of these octahedra of 2/3. The gaps are situated preferentially in the defined octahedral of the mesh with a probability of presence of the gap of 1/3. The cubic system is always preserved but the space group $P4_132$ translates a lowering of symmetry. Its lattice parameter is 0.8346 nm at room temperature (JCPDS card 04-016-4344).
- A totally organized distribution of gaps. The symmetry drops from cubic to tetragonal ($P4_32_12$) and the ordering of the gaps is carried out in a superstructure built on three superimposed meshes (Figure 2C). In some works [2], the space group $P4_32_12$ is indicated instead of $P4_12_12$. This difference translates the direction of rotation chosen for the helical axis $4_3$ or $4_1$ but the structure is identical. The lattice parameters of this structure are a = b = 0.83296 nm and c = 0.83221 nm at room temperature (JCPDS card 04-007-2135).

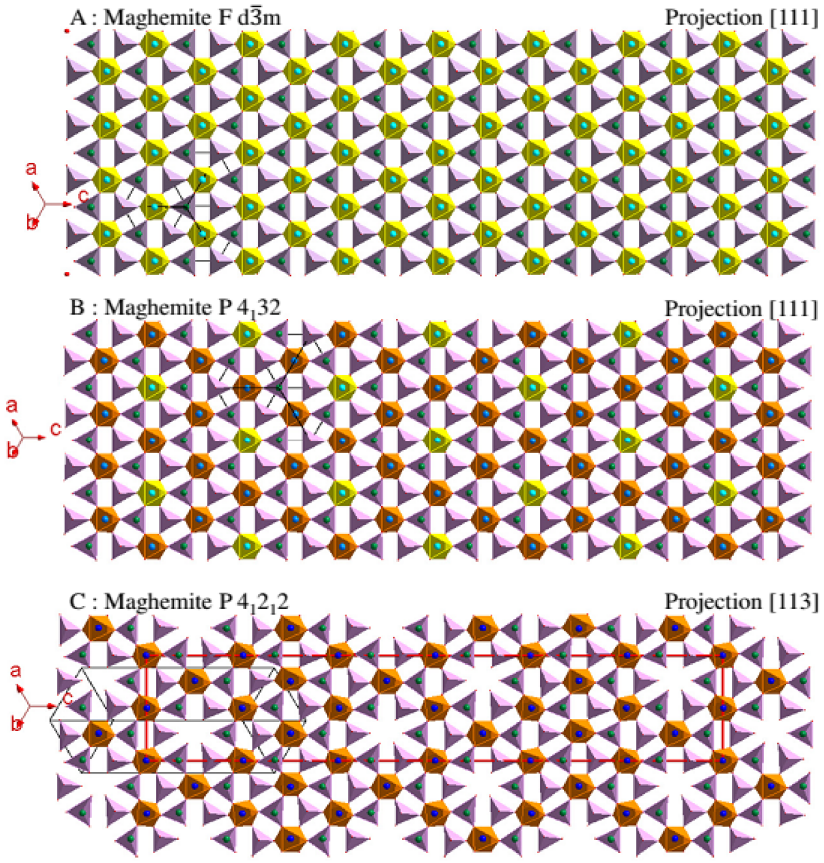


**Figure 2.** (**A**) Projection [111] of maghemite $Fd\bar{3}m$. (**B**) Projection [111] of maghemite $P4_132$. (**C**) Projection [113] of maghemite P $4_12_12$.

The chemical formula of maghemite becomes [4]:

- For the space group $Fd\bar{3}m$: $(Fe^{3+})^{tetra}[Fe^{3+}_{5/3}\square_{1/3}]^{octa}(O^{2-})_4$
- For the space group $P4_132$: $(Fe^{3+}_8)^{tetra}[Fe^{3+}_{4/3}\square_{8/3}Fe^{3+}_{12}]^{octa}(O^{2-})_{32}$
- For the space group $P4_12_12$: $(Fe^{3+}_{24})^{tetra}[Fe^{3+}_{40}\square_8]^{octa}(O^{2-})_{96}$.

### *2.2. Magnetic Properties*

#### 2.2.1. General Information on Magnetism

The magnetic materials are characterized by three main parameters:

- Their magnetic moments ($\vec{\mu}$) which can be assimilated at electric dipoles from orbital atomic moments and spin of materials. Under the effect of an imposed external magnetic field ($\vec{H}$), they tend to line up in the direction of the field which induces a magnetization within the material.
- Their magnetic susceptibility ($\chi$) representing the trend of magnetic moments of the material to be aligned by the presence of an external magnetic field and which can be defined by the magnetization ratio on the external field $\vec{M}/\vec{H}$.
- Their saturation magnetization ($M_s$) representing the maximum value of the magnetization that a material can reach when the external magnetic field increases: it is given for a defined temperature.

Generally, the field is expressed in Oersted, the magnetic susceptibility is not unity and the magnetization is expressed in emu (electromagnetism unit) per gram of sample.

Two big families of magnetic materials exist: the unordered magnetic materials (non-cooperative magnetism) and the ordered magnetic materials (cooperative magnetism).

In the first case, considering the unordered magnetic materials (non-cooperative magnetism), there is no spontaneous arrangement of their magnetic moments and therefor there is neither magnetic order nor spontaneous magnetization. We then differentiate:

- The diamagnetism which is an intrinsic property of the matter such as $\chi < 0$. The magnetic moments with the application of an external field will tend to align in the opposite direction of this field.
- The paramagnetism which is a property due to free electrons of materials or unpaired electrons of ions such as $\chi > 0$. The magnetic moments will tend to align in the direction of an applied external field.

In the second case of ordered magnetic materials (cooperative magnetism), there is a spontaneous arrangement of their magnetic moments $\mu$ even in the absence of an external field. This spontaneous arrangement can be:

- Parallel (ferromagnetism); this results in an overall measurable magnetization for the material even in the absence of an external magnetic field.
- Antiparallel with compensation of magnetic moments (antiferromagnetism); there exist two populations of magnetic moments aligned antiparallel to one another. The two populations of magnetic moments fully compensate and there is no overall magnetization measurable in the absence of an external magnetic field in this type of material.
- Antiparallel without compensation of magnetic moments (ferrimagnetism); a global magnetization is measurable for the material even in the absence of an external magnetic field.

A schematic representation of the five types of magnetic behavior is presented Figure 3.

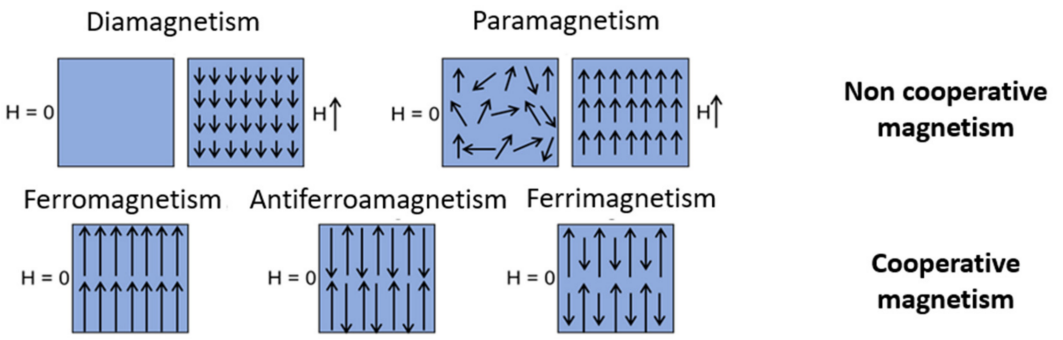


**Figure 3.** Representation of the arrangement of magnetic moments in materials having different magnetic behaviors. When necessary, the behavior with or without the presence of an external field H is specified.

In the three types of cooperative magnetisms, the susceptibility is positive and higher in absolute value than for paramagnetic materials. It should also be noted that the long distance magnetic order is only present for a temperature below a critical value called the Curie temperature ($T_C$) for the ferromagnetism and ferrimagnetism compounds or for a temperature below at the Neel temperature ($T_N$) for the antiferromagnetism materials. If the temperature is higher than one of these two critical temperatures, the thermal agitation becomes enough to suppress spontaneous magnetization and the material then becomes paramagnetic.

Magnetite and maghemite present a ferrimagnetic behavior [5] for the temperatures below the Curie temperature, around 480 °C and 645 °C respectively. The saturation magnetization ($M_S$) are around 92 emu/g for the magnetite and 74 emu/g for the maghemite [6]. These numeric values are reported for massive materials of magnetite and maghemite.

#### 2.2.2. Structuration in Magnetic Areas

In order to decrease the magnetostatic energy (denoted form energy), a material in its massive forms can be divided into magnetic areas denoted Weiss' areas separated by walls denoted Bloch's walls. Inside the Weiss' areas, the spins are antiparallel without compensation of magnetic moments giving rise to magnetization. Due to the variation of magnetization from one area to another, the material does not present macroscopic magnetization without an external magnetic field. Under the effect of a magnetic field, the Bloch's walls will move, widening the areas which present a collinear orientation to the external field. There is a progressive orientation of all the spins of the material. It is often necessary to apply an important external magnetic field around several tesla in order to orient all the magnetic spins of the material in the same direction [7]. This phenomenon is at the origin of the remnant magnetization and of the hysteresis observed when the magnetization $\vec{M}$ of a material is measured as a function of the external magnetic field $\vec{H}$ (Figure 4).

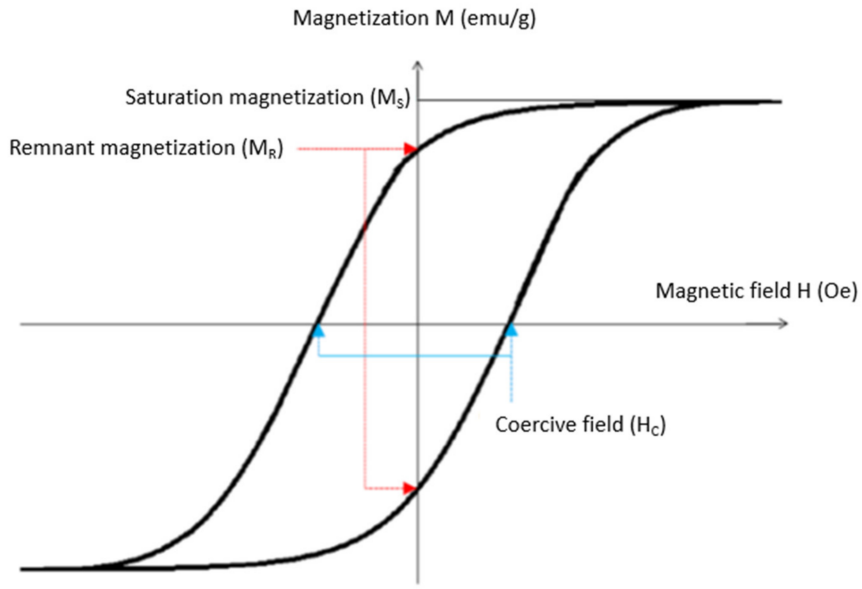


**Figure 4.** Magnetization cycle depending on the field applied for a massive ferro/ferrimagnetic material.

In Figure 4, the magnetization of the material reaches the maximum value $M_S$ (or saturation magnetization) when the imposed field increases enough. All spins are oriented in the same direction. The hysteresis curve also makes it possible to highlight the non-instantaneous nature of the orientation of the magnetic spins within a solid material, thus inducing a delay in magnetization. Two characteristic values of the material can be defined:

- The coercive field ($H_C$) which corresponds to the imposed magnetic field when the magnetization of the material is zero.
- The remnant magnetization ($M_R$) which corresponds to the magnetization of the material when the external field is zero.

2.2.3. Main Sources of Magnetic Anisotropy

Magneto-Crystalline Anisotropy

Within a crystal, the magnetization vector is not isotropic. There are energetically more favorable crystallographic directions for the alignment of magnetic spins. These directions are called axes of easy magnetization. This anisotropy of the crystallographic structure is at the origin of the magnetic anisotropy. The energy required to deflect the magnetization vector with respect to an easy magnetization direction is the magnetocrystalline anisotropy energy denoted $\left(E_{an}^{magn}\right)$ and defined by:

$$E_{an}^{magn} = K_1 V \sin^2\theta + K_2 V \sin^4\theta \quad (1)$$

with $K_1$ and $K_2$ as the anisotropy constants of the material of first order and θ the angle between the direction of magnetization and the easy magnetization direction.

For the magnetite at room temperature, $K_1 = -1.35 \times 10^4$ J·m$^{-3}$, $K_2 = -0.28 \times 10^4$ J·m$^{-3}$ and the easy magnetic direction is the direction [111] [8,9].

For the maghemite at room temperature, $K_1 = -2.5 \times 10^4$ J·m$^{-3}$, $K_2$ is negligible in front of $K_1$ and the easy magnetic direction is the direction [110] [10]. In the case of a mono-domain magnetic particle, the predominant term is the term of order 2 [7] and we reduce the expression of magnetocrystalline anisotropy energy to:

$$E_{an}^{magn} = K V \sin^2\theta \quad (2)$$

Anisotropy of Surface

The magnetic anisotropy of surface is linked to the break of symmetry on the surface of the particles causing the formation of gaps in the crystallographic structure and the decrease of the number of nearest neighbors for the atoms on the extreme surface. An effect now well-known as "spin canting" causes the magnetic spins of atoms on the surface to reorient themselves perpendicular to the latter and thus leads to a significant decrease in the saturation magnetization of the material [11]. This source of anisotropy is more important that the magnetic materials are small because the rate surface/volume increases. This source of anisotropy becomes preponderant in the case of nanoparticles. The energy associated with this anisotropy of surface is written as:

$$E_{an}^{surf} = K_s V \sin^2 \alpha \quad (3)$$

Anisotropy of Shape

The magnetic anisotropy of shape comes from the interaction between magnetic moments within the material and the demagnetizing field specific to any material. In the facts, it will tend, in the case of a material with anisotropic dimensions, to orient the field in the direction of the largest dimension (the magnetization of a cylinder with a negligible section and with an infinite height will be oriented in the direction of the height). For a sphere, this anisotropy is negligible due to a three-dimensional uniformity.

2.2.4. Evolution of Magnetic Properties in the Case of Nanoparticles

The reduction of the size, for example from a 3D material to a 1D or a 0D material, modifies a certain number of magnetic properties. When the size of materials becomes inferior at a critical diameter $D_C$ (Figure 5), the creation of Bloch's walls becomes energy-defeatable and these last disappear to minimize the magnetostatic energy. We then speak of "mono-domain". In the case of nanoparticles, the critical diameter can be calculated by the expression:

$$D_C = 4\,\gamma/\mu_0\,N_{MD}.M_S^2 \quad (4)$$

where $\gamma$ is the energy of creation of a Bloch's wall, $\mu_0$ the vacuum permeability, $M_S$ the saturation magnetization of the material, and $N_{MD}$ the demagnetizing factor for a mono-domain. For mono-domain nanoparticles of magnetite and maghemite, $D_C$ is around 30 nm [7,12].

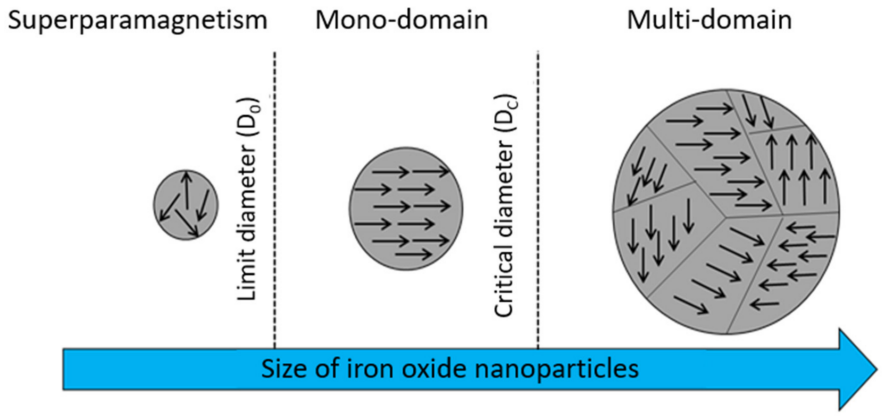


**Figure 5.** Evolution of the magnetic organization of nanoparticles according to their diameters.

Below this critical size, the magnetic properties of magnetite and maghemite nanoparticles also vary. Considering a mono-domain nanoparticle with a diameter below at $D_C$, its magnetic behavior will change depending on the ratio between the total anisotropy energy $E_{an}^{tot}$ and the thermal activation energy $E_{therm}$ with: $E_{an}^{tot} = K_{an}^{tot} \cdot V$ where $K_{an}^{tot}$ is the sum of the magnetocrystalline anisotropy and the surface anisotropy and V the average volume of nanoparticles. $E_{therm} = k_B T$ where $k_B$ is the Boltzmann's constant and T the temperature.

We can distinguish two cases:

- $E_{an}^{tot} > E_{therm}$. The magnetic moments of ferrimagnetic domains are blocked in the easy magnetization direction. A rotation of these magnetic moments by application of an external field then causes the mechanical rotation of the entire nanoparticle. The nanoparticle presents a ferrimagnetic comportment in the case of the magnetite.
- $E_{an}^{tot} < E_{therm}$. The thermal agitation is more important than the total magnetic anisotropy energy and the magnetic moment is free to rotate freely. This magnetic comportment is called superparamagnetism.

Considering these two cases, it is possible to note by the ratio presented in Equation (5) that for a temperature given (for example the room temperature), the direction of the report will depend on the average volume V of nanoparticles and their sizes.

$$E_{an}^{tot} / E_{therm} = K_{an}^{tot} \cdot V / k_B \cdot T \quad (5)$$

If the diameter of the particle is small enough (<$D_0$), the magnetocrystalline anisotropic energy becomes lower than thermal energy at room temperature. The magnetization can then overturn spontaneously and the particle presents a superparamagnetic behavior (Figure 5). For the magnetite and the maghemite, the limit diameter from which nanoparticles present a superparamagnetic behavior is around 20 nm [1,13].

2.2.5. Relaxation Time

When the necessary energy required to return the magnetization becomes lower than the ambient thermal energy, the iron oxide nanoparticles (magnetite and maghemite) show a superparamagnetic behavior. The relaxation time τ corresponding to the inverse of the probability of tilting magnetic spins is then defined by the Néel–Brown law [11]:

$$\tau = \tau_0 \cdot \exp\left(\frac{E_{an}^{tot}}{k_B T}\right) \quad (6)$$

where $\tau_0$ is the characteristic time of relaxation of the order of $10^{-9}$ s [7,9,14,15].

The relaxation time increases when the total anisotropic energy increases and it decreases when the temperature increases. The observation time of the phenomenon is dependent on the characteristic measured time $\tau_m$. We distinguish two cases:

- If $\tau >> \tau_m$, the magnetic moment of the particle appears as blocked and the particle adopts a ferrimagnetic behavior.
- If $\tau << \tau_m$, the magnetic moment of the particle returns around a lot of time during the measure and the average moment is zero. The particle presents a superparamagnetic behavior.

For a given measurement time and a defined volume $V$, the magnetic behavior will depend on the temperature. We can then define the blocking temperature $T_B$ for a particle with a volume $V$ as the temperature at which $\tau = \tau_m$. This blocking temperature can be expressed, if the field is weak or zero, by the relationship:

$$T_B = \frac{K_{an}^{tot} \cdot V}{k_B \ln\left(\frac{\tau_m}{\tau o}\right)} \quad (7)$$

For the magnetic measurements, it is common to take the usual values of $\tau_0 = 10^{-9}$ s and $\tau_m = 100$ s. This equation becomes:

$$T_B = \frac{K_{an}^{tot} \cdot V}{25. k_B} \quad (8)$$

This expression being dependent on the volume of nanoparticles and therefore their diameter, a size distribution within a sample result in a distribution of relaxation times and therefore a distribution of blocking temperature.

Finally, also note that several studies have shown that these equations (Equations (6) and (7)) are not valid only in the case of nanoparticles isolated from each other and without dipolar interactions between them. In fact, these dipolar interactions which can be written according to the Equation (9), when they present within the sample, can be responsible for a shift from the average blocking temperature to high temperature [14–16].

$$E_d = \frac{\mu_0}{4\,\pi\,r^3}\left(\vec{m_1}\cdot\vec{m_2} - \left(3/\mathrm{r}^2\right)\left(\vec{m_1}\,\vec{r}\,\right)\left(\vec{m_2}\,\vec{r}\right)\right) \quad (9)$$

with $\vec{m_1}$ and $\vec{m_2}$ the magnetic moments carried by two nanoparticles and $\vec{r}$ the vector representative of the distance between the two nanoparticles.

The numeric values associated with the magnetic properties of two iron oxide magnetite and maghemite presented in Table 1 are relatively close. These are two ferrimagnetic materials but the presence of cationic gaps in the structure of maghemite causes a decrease in its saturation magnetization. With a controlled size of nanoparticles below the limit diameter $D_0$, these two oxides adopt a superparamagnetic behavior which allows the magnetization of the material to turn spontaneously, opening the way for many applications.

**Table 1.** Summary of the magnetic properties of magnetite and maghemite iron oxides.

| Type of Oxide | Saturation Magnetization | Mono-Domain Critical Diameter | Limit Diameter Superparamagnetism |
|---|---|---|---|
| **Magnetite** | 92 emu/g | $30 \pm 5$ nm | $20 \pm 5$ nm |
| **Maghemite** | 74 emu/g | $30 \pm 5$ nm | $20 \pm 5$ nm |

## 3. Main Synthesis Methods of Magnetite and Maghemite Nanoparticles

Since the first synthesis of magnetic iron oxide nanoparticles in the 1980s, a lot of synthesis methods have been developed (Table 2) to control their sizes and shapes [17–32]. The control of these physicochemical parameters will depend on the synthesis way used. Mastering the separation of germination and growth stages of nanoparticles via the control of pH in the case of coprecipitation (which will be describe in details at the end of this part) [20–23] or the control of temperature in the case of hydrothermal synthesis [24,25,33], by thermal decomposition [28–30] or by polyols process [31,32,34] will allow then the modulation of the size and the shape of nanoparticles. In the case of synthesis by microemulsion [26,27] or by sol-gel process [35,36], the control of the size of nanoparticles is insured by the limitation of the space left for the growth of these.

**Table 2.** Summary of advantages, disadvantages and morphological characteristics and saturation magnetization of the magnetic iron oxide nanoparticles synthesized by the main synthesis methods.

| Method | Advantages | Disadvantages | Shape and Size Saturation Magnetization |
|---|---|---|---|
| **Co-precipitation** [20–23] | - Ferrous and ferric salts, inexpensive reagents<br>- Soft conditions.<br>- Possible large-scale production.<br>- Easy modification surface<br>- Synthesis in aqueous solution. | - Large distribution of size.<br>- Non controlled oxidation.<br>- Low reproducibility.<br>- Aggregation of NPs. | - Sphere 10–55 nm<br>- 16 to 82 emu/g |
| **Hydrothermal Co-precipitation** [24,25] | - Better size control.<br>- Narrow size distribution.<br>- Aqueous solution. | - High temperature.<br>- Long synthesis time.<br>- Possible aggregation of NPs. | - Sphere 12–40 nm<br>- Disk 250–1000 nm<br>- 53 to 82 emu/g |

**Table 2.** *Cont.*

| Method | Advantages | Disadvantages | Shape and Size Saturation Magnetization |
| --- | --- | --- | --- |
| **Micro-emulsions** [26,27] | - Better size control.<br>- Narrow size distribution.<br>- Adjustable size and shape.<br>- Isolated particles. | - Low yield.<br>- Poor crystallinity.<br>- Difficulties in washing surfactants. | - Cube, sphere 2–30 nm<br>- Needles 20–80 nm |
| **Thermal decomposition** [28–30] | - Narrow size distribution.<br>- High crystallinity.<br>- Isolated particles. | - Organic solvents.<br>- High temperature.<br>- Phase transfer required if application in aqueous solution.<br>- Low yield. | - Cube, sphere, triangle, tetrapode.<br>- 3–500 nm<br>- 20 to 82 emu/g |
| **Polyol method** [31,32] | - Reduction of metallic salts.<br>- Narrow size distribution.<br>- Isolated particles. | - High temperature.<br>- Difficulties in washing surfactants. | - Sphere 6–100 nm<br>- 50 to 69 emu/g |
| **Sol-gel** [35,36] | - Soft conditions.<br>- Narrow size distribution.<br>- High crystallinity. | - Long synthesis time.<br>- The solid matrix can be difficult to eliminate. | - Sphere 4–200 nm<br>- 47 to 62 emu/g |

### *3.1. Hydrothermal Synthesis*

The method called hydrothermal [24,25,33] based on the precipitation of nanoparticles from ferrous and ferric precursors by elevation of pH was developed in the 1990s. A mix of ferrous ions, ferric ions and a basis is sealed in a hydrothermal bomb and placed in the oven for a period time ranging from several hours to several days. This treatment allows to obtain magnetic iron oxide nanoparticles better crystallized and generally having medium size around 15 to 1000 nm (Table 2). It is also possible to improve the crystallinity of nanoparticles previously synthesized owing to a hydrothermal treatment.

### *3.2. Synthesis by Microemulsion*

The synthesis method called "by microemulsion" is sometimes called reverse micelle precipitation [26,27]. The principle is to synthesize nanoparticles in a confined space in order to control better their size. These confined spaces are here micro drops of aqueous solution surrounded by a monolayer of surfactants allowing the dispersion of nanoparticles in an organic phase as cyclohexane, for example in the works of Z.H. Zhou et al. [26]. The ferric and ferrous precursors are dissolved in water micro drops of a first two-phase solution (aqueous phase/organic phase) whereas the basis is dissolved in micro-drops of a second two-phase solution (aqueous phase/organic phase). The vigorous mixture of the two two-phase solution will then promote their contact. It is during the contact between micro-drops that the precipitation of nanoparticles in a confined environment will take place. This method allows to obtain iron oxide nanoparticle with a good dispersion in organic phase, spherical, cubical, or in needles and between 2 and 80 nm (Table 2).

### *3.3. Thermal Decomposition*

The thermal decomposition is another synthesis method of oxide nanoparticle which is particularly developed since the 2000s [28–30]. Its principle rests on the decomposition of organometallic precursors (for example iron oleate or iron stearate for the synthesis of iron oxide nanoparticles) [30] within an organic solvent with a high boiling point [30] and in the presence of a surfactant stabilizing agent [30]. A definite interest of this synthesis method is the tight control of the size from 3 to 500 nm. The shape of iron oxide nanoparticles can also be controlled (spheres, cubes, bipyramids, tetrapods, . . . ) (Table 2). On the other hand, this method requires the use of organic solvents and therefore washing procedures and exchange of complex ligands for applications in aqueous solution.

### *3.4. Polyols Methods*

The so-called "polyols" synthesis method is based on the last method on decomposition by increasing the temperature of the ferric precursor (generally iron III acetylacetonate) [31,32,34]. It consists of hydrolysis at high temperature of the ferric precursor within a polyols environment (ethylene glycol, di(tri/tetra) ethylene glycol). These polyols serve both as solvent, reducer agent, reducing a part of $Fe^{3+}$ ions from the $Fe^{2+}$ precursor and surfactants stabilizing nanoparticles formed during the synthesis. The isolated iron oxide nanoparticles obtained by this method are spherical and measure between 6 and 100 nm (Table 2). This method can also be carried out in a bomb, we then speak solvothermal polyol method [37].

### *3.5. Sol-Gel Process*

The Sol-gel process is another method developed since the 1990s [35,36]. It involves hydrolyzing a metallic alcoxyde solution to obtain a colloidal solution (denoted "sol") then condensing and polymerizing to obtain a wet gel. It is by drying and crushing this gel that the nanoparticles are obtained, often after an annealing step to eliminate the organic matrix. This synthesis can then be assisted by microwaves to obtain nanoparticles better crystallized [38] and precisely of controlled size from 4 to 200 nm. It is however difficult to eliminate the solid matrix residues (Table 2).

### *3.6. Synthesis by Co-Precipitation*

The co-precipitation is the first synthesis method of nanoparticles developed by R. Massard in the 1980s [20], and still currently the most used [14,21,39–49] by researchers working on magnetic iron oxide nanoparticles. It is based on joint precipitation in aqueous solution of ferric and ferrous ions by addition of a basis such as ammoniac or sodium hydroxide. The main advantages of this method are that it is easy to implement, even on a large scale, and to allow the synthesis of nanoparticles with a quasi-spherical shape and with a size ranging from 10 to 100 nm directly in aqueous solution (Table 2). However, this method is not without disadvantages. There is often an aggregation if nanoparticles with this method at neutral pH and the control of the size stay limited.

The ferrous $Fe^{2+}$ and ferric $Fe^{3+}$ cations are stable in acid solution and precipitate when the basicity of the solution increases to form iron oxide by the Equation (10) [3]:

$$Fe^{2+}{}_{(aq)} + 2\ Fe^{3+}{}_{(aq)} + 8\ OH^{-}{}_{(aq)} \rightarrow Fe_3O_{4(s)} + 4\ H_2O_{(l)} \quad (10)$$

However, due to high surface reactivity and their small sizes, the synthesized iron oxide nanoparticles will be able to partially oxidize to maghemite in the presence of oxygen according to the Equation (11):

$$4\ Fe_3O_{4(s)} + O_{2\ (g)} \rightarrow 6\ \gamma\text{-}Fe_2O_{3(s)} \quad (11)$$

The formation of nanoparticles during the synthesis by co-precipitation takes place in four stages, as described by the V.K. Lamer model [50] (Figure 6):

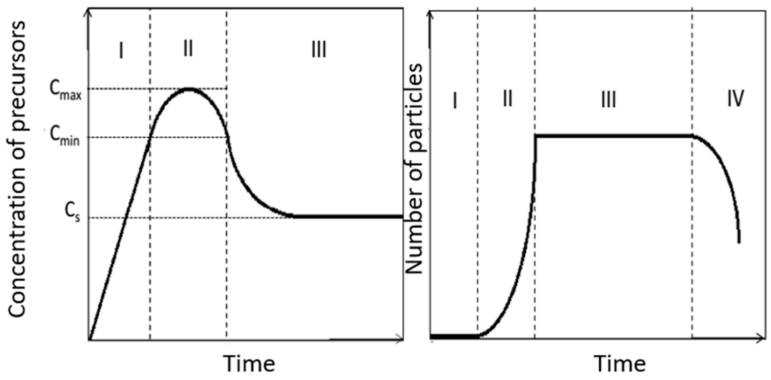


**Figure 6.** Lamer diagrams representing the concentration of aqua-hydroxo precursors complexes as well as the number in the reaction as a function of time. We can distinguish on these diagrams the different stages of the reaction.

- Stage I: Formation by inorganic polycondensation of zero charge aqua-hydroxo complexes whose concentration will increase with the pH of the solution: $[Fe_2(OH)_4(H_2O)_8]^0$ for the $Fe^{2+}$ ions and $[Fe_2(OH)_6(H_2O)_6]^0$ for the $Fe^{3+}$ ions.
- Stage II: Nucleation which begins when the concentration of precursors reaches a critical value of saturation ($C_{min}$). There is then appearance of germs in the solution. These germs, very small, tend to redissolve easily. The quick germs formation and redissolution process will continue whereas the concentration of precursors increases. When the critical threshold is reached, stable germs are created and there follows a sudden decrease in concentration of precursors in the solution. If the concentration of precursors falls below the minimum value ($C_{min}$), the formation of new germs is blocked.
- Stage III: Growth of stable germs on the solution. It is carried out by addition of precursors in surface of germs by olation/oxolation. The growth will continue if the concentration of precursor is greater than the solubility of the solid (nanoparticles) in the solution. It should be noted that recently, D. Faivre et al. [51] proposed a growth model of magnetite nanoparticles. According to this model, primary nanoparticles around the nanometer size will be formed at an intermediate stage. These nanoparticles will aggregate then to form the finals nanoparticles.
- Stage IV: Ripening. This is the last important step for the final characterization of the synthesized nanoparticles. A restructuring of nanoparticles formed by the crystallization of hitherto amorphous phases can occur during this stage. The possible aggregation of nanoparticles as well as the Ostwald ripening during which the smallest nanoparticles are dissolved in favor of the larger ones can also intervene during this stage. These two processes are both driven by the reduction of the surface energy of nanoparticles.

Considering the V.K. Lamer model [50], it appears that the marked separation between the phase II and III, i.e., between the nucleation and the growth is an essential factor for the control of the size of the obtained nanoparticles. It is therefore preferable that the nucleation step is very short so that all the germs are generated at the same time and the next stage of growth is longer. In fact, considering a closed system, the number of germs obtained during the nucleation phase will determine the number of particles which can grow. The size of particles obtained at the end of the phase III will be determined by the quantity of precursors initially introduced by the number of germs formed in phase II.

Another way to better control the size of nanoparticles obtained at the end of the synthesis involves limiting the effect of phase IV, in particular by limiting the Ostwald ripening. E.C. Vreeland et al. [52] compensated for the consumption of precursor required for the growth of nanoparticles by adding precursor continuously during the synthesis. They thus maintained the constant concentration of the precursor (located between $C_{min}$ and $C_S$) so that neither subsequent nucleation nor Ostwald ripening occurs. The nanoparticles growth is predictable, which makes it possible to obtain nanoparticles of the desired size.

The shape and the size of nanoparticles obtained by co-precipitation can be adjusted relatively effectively by controlling the parameters of the synthesis.

R. Massart, V. Cabuil et al. [21,53], one of the pioneers of this synthesis method of magnetic iron oxide nanoparticles, have carried out in-depth studies on the influence of different parameters such as the basis used ($NH_4OH$, $CH_3NH_2$, NaOH, KOH), the pH of precipitation, the adding of cations in the solution ($N(CH_3)_4^+$, $CH_3NH_3^+$, $Li^+$, $Na^+$, $K^+$, $NH_4^+$), and the effect of $Fe^{2+}/Fe^{3+}$ ratio on the size and polydispersity of synthesized nanoparticles. They have shown in particular that, by adjusting these parameters, they can obtain samples with a controlled size between 4.2 and 16.6 nm. They also highlighted that certain conditions, especially the ratio of $Fe^{2+}/Fe^{3+}$ introduced and the precipitation pH of nanoparticles, can affect the formation of a second phase constituted of oxohydroxide $\alpha$-FeOOH, denoted goethite, non-magnetic in addition to the magnetic oxides.

J.P. Jolivet, E. Tronc et al. [23,54] also studied that the synthesis parameters can influence the size and the monodispersity of nanoparticles. They have shown in particular that by adjusting the ionic force of the solution during the synthesis of nanoparticles by co-precipitation, they can obtain nanoparticles with a controlled size between 2 and 15 nm. They were able to define the best conditions to obtain batches of particles of uniform size, i.e., a pH of precipitation between 8.5 and 12.0 and an ionic force of the solution between 0.5 and 3.0 $mol{\cdot}L^{-1}$. This team also extended the studies around the influence of the ration $Fe^{2+}/Fe^{3+}$ on the yield of magnetic materials. They have shown that for a ratio of 0.3, the two phases that are the maghemite/magnetite mixture and the goethite coexisted; for a ratio higher than 3.5, the goethite is not present but the magnetite formed is not stoichiometric; for a ratio of 0.5, the magnetite approaches stoichiometry and the size and the composition of nanoparticles become more homogeneous.

Parallel to this marked influence of the molar ratio $Fe^{2+}/Fe^{3+}$ on the composition of nanoparticles formed, L. Babes et al. [55] observed that the average size of nanoparticles increases with the ratio $Fe^{2+}/Fe^{3+}$. They also established that the nanoparticles formed kept interesting magnetic properties only for molar ratios $Fe^{2+}/Fe^{3+}$ between 0.4 and 0.6.

On the other hand, D.K. Kim et al. [56] showed that the presence or absence of oxygen in the reaction medium affects the size of the nanoparticles obtained. In fact, the particles obtained during a synthesis under nitrogen are relatively smaller than those obtained during a synthesis under air.

In conclusion, the synthesis of iron oxide nanoparticles by co-precipitation is a synthesis method allowing to quickly obtain a large quantity of nanoparticles. It is simple in its implementation, but its parameters are complex. It presents the potential to produce nanoparticles in aqueous solution and without toxic solvent. By adjustment of several parameters of synthesis, it is possible to obtain nanoparticles of desired composition and size.

However, if the monodispersity of samples can be improved by adjusting the synthesis parameters, the latter remains less good than for other more complex synthesis complex (the thermal decomposition for example). In addition, the synthesized nanoparticles have a strong tendency toward aggregation in aqueous solution without further treatment. This trend will considerably limit the possible applications, especially in the biomedical field.

These two mains defects that are the polydispersity and the aggregation of nanoparticles obtained could be limited by the stabilization of nanoparticles in aqueous solution. The functionalization of iron oxide nanoparticles by adding a ligand during the synthesis or after it in order to stabilize them in aqueous solution will be the subject of the end of this review.

### *3.7. Synthesis by Microwave*

Heating using microwave has become more and more popular in the past few years [38,57–59]. Owing to the microwave irradiations, the molecules on the sample will line up according to the applied field. This forced movement will thus allow internal heating of the sample. Unlike conventional heating, there will therefore be no temperature gradient on the sample

with microwave heating. In addition, the microwave irradiation will allow a time reduction of the synthesis [60].

Synthesis assisted by microwave allows to obtain nanoparticles with a controlled size and shape [61–63]. The various methods which have been mentioned above can be assisted by microwaves. In fact, thermal decomposition [57], hydrothermal synthesis [64], sol-gel process [38], co-precipitation [65] use heating by microwaves.

## 4. Main Washing and Size Selection Methods for Nanoparticles

Since the synthesis of nanoparticles for various applications has developed, a number of washing procedures (or purification) of nanoparticles have also been developed. These processes have sometimes a second goal consisting in the fractionation of nanoparticles in function of their size or the deletion of possible aggregate in addition to another undesirable elements [66–69]. In this part, the main existing method relating to washing and sorting by size of magnetic iron oxide nanoparticles will be presented considering their principles and main mechanisms as well as their respective characterizations.

### *4.1. Dialysis*

The purification by dialysis is a purification method often used, particularly in biochemistry. It consists of placing the sample to be purified in a dialysis tube constituted of a semi-permeable membrane only allowing the passage of molecules whose molecular weight is less than a certain value (denoted cutoff threshold). This dialysis tube is then introduced to a container of ultra-pure water with a volume superior than the volume of the tube (generally 100 to 1000 times higher). Under the effect of the chemical species concentration gradient (such as molecules of free ligand or ions derived of precursors) existing on both sides of the membrane, the sufficiently small species will migrate through the membrane and diffuse in order to distribute themselves uniformly throughout the available volume. So, the concentration of impurities to be removed in the tube containing the sample is divided by a factor corresponding to the factor between the volume of the dialysis tube filled with sample and the total volume of the container of ultra-pure water. The purification of the sample can be improved by the repetition of this handling. This washing method is often considering one of the least aggressive methods for samples because it does not involve significant physical stress or difficulties in recovering the sample after purification. However, it is time-consuming (the diffusion is a slow process, they last several days) for small sample volumes processed. In a recent work, L.K. Mireles et al. [70,71] showed that the purification of iron oxide nanoparticles by this method, yet considered "sweet", caused changes in the surface chemistry of nanoparticles. In addition, A. Lassenberger et al. [71] also showed that the dialysis of iron oxide nanoparticles for 72 h caused a decrease in the ratio of ligands at the surface which generated the aggregation of nanoparticles.

### *4.2. Centrifugation*

The classical centrifugation is one of the most used methods for the washing of nanoparticles [68,69]. It involves inserting the sample into the centrifuge tubes and applying an extremely rapid rotation movement. Under the effect of the centrifugal force, the heaviest objects of the solution (generally the nanoparticles that we want to purify) accumulate at the base of the tubes while the parasites ions and the ligand in excess will remain in solution in the supernatant. The washing by centrifugation is generally carried out by a succession of several centrifugation phases followed by re-solution of the nanoparticles accumulated at the base of the tubes. By adjusting the speed of the rotation of the centrifugation as well as the time of centrifugation, it is possible to make size selection on the sample of nanoparticles we want to increase the monodispersity. This method is simple to implement and allows to remove ions and molecules of free ligands from the samples. However, the high physical stress inflicted on nanoparticles and the succession of the forced aggregations they undergo can lead to a decrease in the colloidal stability of samples if the centrifugation phases are very fast (in rotation speed) or longer (in time). In addition, any aggregate

formed during the synthesis will be recovered in the pellet unless a first centrifugation with a low speed is carried out to eliminate them from the sample.

### 4.3. Centrifugation with Viscosity Gradient

This type of washing by centrifugation is based on the same principle as that of the classical centrifugation, but splitting the sizes of nanoparticles present in solution owing to a viscosity gradient in the solution. This time the sample is introduced into the upper part of a tube prepared beforehand by adding a succession of liquids of decreasing density and viscosity starting from the bottom of the tube. This succession of adding aims to obtain a partially filled tube and presenting a viscosity gradient from the bottom of very viscous tube to the top of the tube where the viscosity is close to that of water. This succession of density liquids and decreasing viscosity can be obtained for example by the mixture water/polyvinylpyrrolidone (PVP) [72] having a decreasing mass percentage of PVP over the addition or by the mixture water/ethylene glycol (EG) [73] starting to fill the tube with pure EG to finish with pure water. This modification of this method allows to separate more efficiently the population of different sizes within a sample, the largest nanoparticles, heavier, sinking further in the liquid with a higher viscosity. This improved method provides better results in terms of size selection than the classical centrifugation. However, the advance preparation of tubes makes it much more complex and time-consuming to apply (in particular if several successive centrifugations are necessary). In addition, it is sometimes difficult to recover the nanoparticles present in the liquid phases with high viscosity and completely eliminate these viscous liquids of the sample.

### 4.4. Ultrafiltration

The washing and the size split of nanoparticles by ultrafiltration consists in passing nanoparticles through a porous membrane with a controlled pore size thus allowing only the species with a molecular weight below a membrane-specific limit (denoted cutoff threshold) [66,69,74,75]. The gravity only can allow the passage of the solution through the membrane. A slight overpressure imposed on the upper part of filtration device can be applied. This method can be used simultaneously with the centrifugation using specific centrifuge tubes with porous membrane. This method, mostly when it is coupled with the centrifugation, allows to eliminate in the sample small molecules or ions which can pass through the membrane. On the other hand, as in the case of dialysis, Lassenberger et al. [71] showed that the ligand ratio (PEG) in surface of NPs were drastically reduced by the repetition of ultrafiltration, which result the quick aggregation of nanoparticles in solution. In addition, we can see with this method a loss of a part of the nanoparticles which remain attached to the surface of the membrane; nanoparticles that are difficult to recover.

### 4.5. Size selection Precipitation (SSP)

The washing and size fractionation method denoted SSP “size selection precipitation” can be applied jointly with other methods such as the magnetic separation or the centrifugation. It rests by destabilization of nanoparticles in solution by adjusting different factors. The destabilization of nanoparticles can be performed by adjusting pH of the solution [21], the ionic force by adding ions in solution [76] (such as chloride ions) or the mixture between good and bad solvents which will depend on the surface functionalization of the nanoparticles to be sorted. If the destabilization of nanoparticles is enough, nanoparticles can flocculate or aggregate becoming easy to recover by classical filtration. It is possible to observe a transition denoted “liquid-gas” with the appearance of two distinct phases in the solution [21,76,77]; the most concentrated lower phase will contain the biggest nanoparticles. The adjustment of parameters (pH, ionic force, nature of solvent, . . . ) cannot be enough to totally destabilize the nanoparticles. A partial destabilization can however favor the purification of nanoparticles by methods such as centrifugation or magnetic separation.

### 4.6. Extraction

The extraction is a method widely used in organic chemistry to separate species having different affinities with two given solvents (generally an apolar organic solvent and water). Unlike SSP by mixing solvents whose purpose was only to modify the stability of nanoparticles to provoke their flocculation, the two selected solvent must not be miscible and must form two separate phases (water/chloroform for example) [66,78,79]. The nanoparticles are scattered in one of the two phases of the mixture after agitation and decantation, while the impurities will stay in the second phase. In the case of functionalized iron oxide nanoparticles by ligands in surface, the affinity with a solvent or another will be due essentially to the nature of ligands which cover them. So functionalized nanoparticles by oleic acid or other ligands with long carbon chains will tend to migrate to the organic phase constituting an apolar solvent while functionalized nanoparticles by small charged molecules such as citrate will migrate to the aqueous phase, a polar solvent. This washing method is simple to perform and is mainly used for purifying nanoparticles whose functionalization stabilize them in organic solvent. The synthesized residues will be solubilized in the aqueous phase.

### 4.7. Magnetic Separation

Magnetic separation is by definition only used for magnetic nanoparticles. It attracts nanoparticles within a solution via the application of a magnetic field (often via a permanent magnet) [67,77,80,81]. The largest nanoparticles will be easy to attract with a magnetic field, especially if they are agglomerated in the form of a cluster. The smallest nanoparticles which are totally isolated and stabilized in the solution by surface ligands will be more difficult to attract. The size sorting of nanoparticles by this principle can be done by modulation of exposure time of the sample to the magnetic field (for example, a short exposition of a few seconds will aim only to remove the big aggregates of the solution). In the case where the field will not be provoked by a permanent magnet but by an electromagnet, a modulation of the power of the magnetic field is possible to attract nanoparticles with a given minimum size [80,82]. One of the advantages of this separation and washing method is it is very easy to implement and effective to eliminate free ions and ligands in excess. It also allows the elimination of any nonmagnetic by-products which can appear during the synthesis of iron oxide nanoparticles in production conditions (such as hydroxides or oxohydroxides). In a recent work, Lassenberg et al. [71] showed that during washing by repeated magnetic separation of the same sample of nanoparticles, the ligands ratio in the sample will tend to decrease significantly during the first washing, sign of the elimination of free ligands. However, unlike washing by dialysis and filtration that they have experienced too, the ligands ratio in the sample stabilizes after the first washing at a sufficiently high value to keep the stability of nanoparticles in the solution and avoid the aggregation.

## 5. Stabilization of Magnetite and Maghemite Nanoparticles in Solution

### 5.1. Iron oxide Nanoparticles Behaviour in Solution

As we saw earlier, the magnetic iron oxide nanoparticles from the coprecipitation will tend to aggregate in aqueous solution at neutral pH. The breaking crystal continuity at the surface of the iron oxide nanoparticles reveals iron atoms with partial charges. These surface atoms behave as Lewis acid and will be able to react with electron donors. So, surface iron ions will bond in the aqueous solution with the atoms of water [21] which dissociate to form a hydroxide layer at the surface of nanoparticles. In function of the pH of the solution, the hydroxide groups -OH protonate in groups $OH_2^+$ or deprotonate in groups $-O^{-1}$. So, the surface of iron oxide nanoparticles will be positively charged, negatively charged, or neutral in the function of the pH of the solution. The isoelectric point, i.e., the pH value which the surface of iron oxide nanoparticles is electrically neutral in aqueous solution is between 6.8 and 7.4 [21,83]. Around these pH values, ($5.0 < pH < 9.0$), the surface charge of nanoparticles is no longer important enough for the electrostatic repulsions, preventing their aggregation under the effect of Van der Waals forces. The iron oxide nanoparticles lose their stability in water and flocculate. Since most biological applications require stable

nanoparticles at pH ≈ 7, the aggregation by functionalizing their surface by organic ligands or inorganic shells should be limited, thus increasing the inter-particle repulsions.

### *5.2. Main Stabilization Methods*

The surface functionalization of magnetic iron oxide nanoparticles can have two separate objectives: on the one hand, the stabilization of nanoparticles to avoid their aggregation in a given solution, on the other hand, the desire to make these nanoparticles functional for a given application. In this part, we will only deal with surface functionalization of nanoparticles. Generally, the stabilization of nanoparticles in solution goes through the creation of repulsions between particles. The two main types of repulsions which can be induced by the surface functionalization of nanoparticles are electrostatic repulsions and the repulsions by steric hindered.

The electrostatic repulsions can be induced by grafting of small charged molecules, the encapsulation in liposomes constituted of a double layer of surfactants having a charged head or the use of other inorganic materials such as silica or gold. The repulsion by steric hindered can be induced by grafting in surface of polymers nanoparticles either by simple adsorption or by grafting of the polymer via a terminal function.

The main types of functionalization (Figure 7) described in the literature are [84]:

- The functionalization by adsorbed polymers such as dextran [85,86], PVA [87,88] or chitosan [89,90].
- The functionalization by small charged molecules such as carboxylates [91,92], phosphonates [93], or sulfonate [94].
- The functionalization by inorganic shell most of the time noble metals such as silver and gold [95] or silica [96,97].
- The functionalization by grafted polymers by the terminal functions such as PEG-COOH [98,99] or polyethylenimine [100].
- The encapsulation in liposomes in the case of a double layer of fatty acids (oleic acid for example) [101].

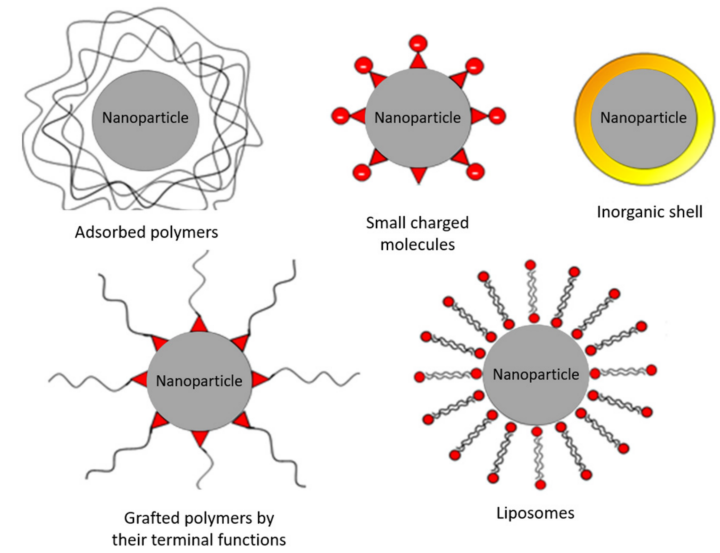


**Figure 7.** Representative schema of the main modes of functionalization of magnetic iron oxide nanoparticles.

### *5.3. Stabilization by Citrate Ligands*

Citrates are part of the first molecules for the stabilization of iron oxide nanoparticles [48,49,91,102]. Citric acid is a tricarboxylic acid α-hydroxylated with chemical formula $C_6H_8O_7$ (M = 192 g·mol$^{-1}$) and showing no toxicity to mammals [103]. Commonly used as an acidifier in the food industry, it also produced in all cells of all aerobic organisms during the Krebs cycle by condensation of oxaloacetate and acetyl-coenzyme A. Citric

acid is a weak triacid which therefore has three separate pKa: there also are four different predominant forms in function of pH (Figure 8).

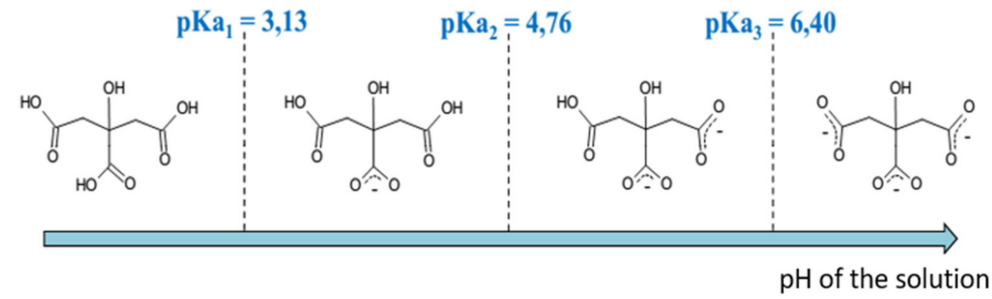


**Figure 8.** Evolution of the predominant species of citric acid as a function of the evolution of the pH of the solution.

If the pH of the solution is below than $pKa_1$, the fully protonated citric acid is the specie which predominates in solution, with the increase of pH, the carboxylic acid groups will gradually deprotonate into carboxylates to the citrate form when the pH is higher than pKa [2]. Citrate ions will be able to adsorb via one or two carboxylate functions on the surface of iron oxide nanoparticles. The negatively charged carboxylate functions not linked to the surface of the nanoparticles and on the periphery of the functionalized nanoparticles will cause electrostatic repulsions preventing the aggregation of the nanoparticles. This principle of stabilization of nanoparticles at pH 7 by carboxylic acids is commonly used in the literature [104]. Several modes of interactions between citrates and nanoparticles depending on the number of complex carboxylate groups and the type of interaction between the group and the surface on the nanoparticles can be envisaged (Figure 9).

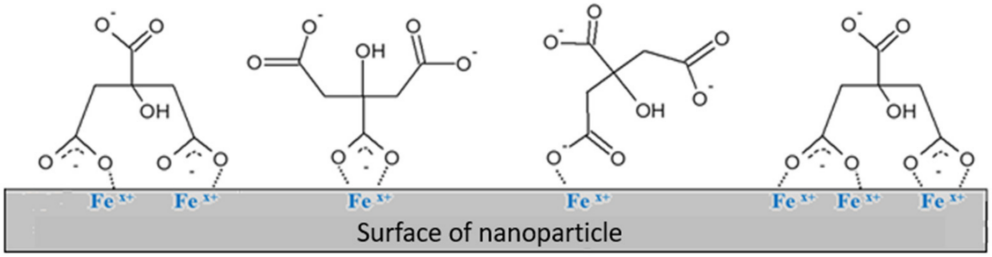


**Figure 9.** Schema several possible binding modes between the citrate ligands and the surface an iron oxide nanoparticle.

When the iron oxide nanoparticles are functionalized by citrates, the isoelectric point for which the aggregation of nanoparticles occurs drop from pH 7 for bare nanoparticles to pH 5 [21]. The functionalized nanoparticles are stabilized and do not aggregate at physiological pH, which greatly facilitate their use in the biological field. The use of citrates as ligands is not limited to the only stabilization of nanoparticles. By their many free functional groups -COOH in solution, they can be used to support a future functionalization. Bishop et al. [105] changed for example citrates to replace the hydroxide group by an alkyl, thus paving the way for future modifications through the Huisgen cyclo-addition reaction or denoted as "click-chemistry" [106].

## 6. Conclusions

Considering the bibliographic considerations set out in this review, structural and magnetic properties of iron oxides nanoparticles, several synthesis ways and purification methods have been described. As a function of applications, different synthesis and washing methods are pertinent. For example, the synthesis method by co-precipitation allowing to get directly magnetic iron oxide nanoparticles in aqueous solution is a good

solution for the biological fields and application as contrast agent for magnetic resonance imaging. In order to overcome certain defects inherent in this method of synthesis such as the strong tendency of synthesized nanoparticles to aggregate, this method can be modified by the adding of ligands in the solution. The citrate ligand described in this review can be used because it has a strong affinity toward the surface of iron oxide nanoparticle and for its no-toxicity. In order to improve the reaction yield and to increase the monodispersity of the solution, one-step microwave heating can be envisaged.

**Author Contributions:** Writing review, T.G., P.V. and S.F.; Supervision, H.M., J.-C.D., F.C. and S.F. All authors have read and agreed to the published version of the manuscript.

**Funding:** This research received no external funding.

**Informed Consent Statement:** Not applicable.

**Conflicts of Interest:** The authors declare no conflict of interest.

## References

1. Teja, A.S.; Koh, P.-Y. Synthesis, properties, and applications of magnetic iron oxide nanoparticles. *Prog. Cryst. Growth Charact. Mater.* **2009**, *55*, 22–45. [CrossRef]
2. Basly, B. Conception et Caractérisation de Nano-Objets Magnétiques Pour L'imagerie par Résonance Magnétique (IRM). Strasbourg. 2010. Available online: http://theses.unistra.fr/ori-oai-search/notice.html?id=oai:EPrintsUneraTest01:2113&printable=true (accessed on 15 July 2022).
3. Bragg, W.H. The Structure of Magnetite and the Spinels. *Nature* **1915**, *95*, 561. [CrossRef]
4. Baaziz, W. Synthèse et Caractérisation des Nanoparticules Spinelles et Coeur-Coquille à Base D'oxyde de fer et de Cobalt. Starsbourg. 2011. Available online: https://www.semanticscholar.org/paper/Synth%C3%A8se-et-caract%C3%A9risation-des-nanoparticules-et-%C3%A0-Baaziz/2c604493355223c8a21532718b63438a6ea8ee43 (accessed on 15 July 2022).
5. Schwertmann, U.; Cornell, R.M. *Iron Oxides in the Laboratory: Preparation and Characterization*; Wiley-VCH: Hoboken, NJ, USA, 2000.
6. Ho, D.; Sun, X.; Sun, S. Monodisperse Magnetic Nanoparticles for Theranostic Applications. *Acc. Chem. Res.* **2011**, *44*, 875–882. [CrossRef] [PubMed]
7. Hillion, A. Études des propriétés magnétiques d'assemblées de nanoparticules de Co, FeRh et FeAu. Ph.D. Thesis, Claude Bernard University Lyon 1, Villeurbanne, France, 5 October 2012.
8. Skumryev, V.; Blythe, H.J.; Cullen, J.; Coey, J.M.D. AC susceptibility of a magnetite crystal. *J. Magn. Magn. Mater.* **1999**, *196*, 515–517. [CrossRef]
9. Ozdemir, O.D.D. *Rock Magnetism: Fundamentals and Frontiers*; Cambridge University Press: Cambridge, UK, 1997.
10. Valstyn, E.; Morrish, A.; Hanton, J. Ferromagnetic Resonance of Single-Domain Particles. *Phys. Rev.* **1962**, *128*, 2078. [CrossRef]
11. Neel, L. Anisotropie Magnetique Superficielle Et Surstructures Dorientation. *J. Phys. Radium* **1954**, *15*, 225–239. [CrossRef]
12. Zijlstra, H. Permanent magnet; theory. In *Ferromagnetic Materials*; Wohlfarth, E.P., Ed.; North Holland: Amsterdam, The Netherlands, 1982; Volume 3.
13. Chatterjee, J.; Haik, Y.; Chen, C.-J. Size dependent magnetic properties of iron oxide nanoparticles. *J. Magn. Magn. Mater.* **2003**, *257*, 113–118. [CrossRef]
14. Sreeja, V.; Joy, P.A. Effect of inter-particle interactions on the magnetic properties of magnetite nanoparticles after coating with dextran. *Int. J. Nanotechnol.* **2011**, *8*, 907–915. [CrossRef]
15. Sreeja, V.; Jayaprabha, K.N.; Joy, P.A. Water-dispersible ascorbic-acid-coated magnetite nanoparticles for contrast enhancement in MRI. *Appl. Nanosci.* **2015**, *5*, 435–441. [CrossRef]
16. Jayaprabha, K.N.; Joy, P.A. Citrate modified beta-cyclodextrin functionalized magnetite nanoparticles: A biocompatible platform for hydrophobic drug delivery. *Rsc. Adv.* **2015**, *5*, 22117–22125. [CrossRef]
17. Laurent, S.; Forge, D.; Port, M.; Roch, A.; Robic, C.; Elst, L.V.; Muller, R.N. Magnetic iron oxide nanoparticles: Synthesis, stabilization, vectorization, physicochemical characterizations, and biological applications. *Chem. Rev.* **2008**, *108*, 2064–2110. [CrossRef] [PubMed]
18. Gupta, A.K.; Gupta, M. Synthesis and surface engineering of iron oxide nanoparticles for biomedical applications. *Biomaterials* **2005**, *26*, 3995–4021. [CrossRef] [PubMed]
19. Sheng-Nan, S.; Chao, W.; Zan-Zan, Z.; Yang-Long, H.; Venkatraman, S.S.; Zhi-Chuan, X. Magnetic iron oxide nanoparticles: Synthesis and surface coating techniques for biomedical applications. *Chin. Phys. B* **2014**, *23*, 037503.
20. Massart, R. Preparation of Aqueous Magnetic Liquids in Alkaline and Acidic Media. *IEEE Trans. Magn.* **1981**, *17*, 1247–1248. [CrossRef]
21. Lefebure, S.; Dubois, E.; Cabuil, V.; Neveu, S.; Massart, R. Monodisperse magnetic nanoparticles: Preparation and dispersion in water and oils. *J. Mater. Res.* **1998**, *13*, 2975–2981. [CrossRef]

22. Lee, J.; Isobe, T.; Senna, M. Preparation of ultrafine Fe3O4 particles by precipitation in the presence of PVA at high pH. *J. Colloid Interface Sci.* **1996**, *177*, 490–494. [CrossRef]
23. Vayssieres, L.; Chaneac, C.; Tronc, E.; Jolivet, J.P. Size tailoring of magnetite particles formed by aqueous precipitation: An example of thermodynamic stability of nanometric oxide particles. *J. Colloid Interface Sci.* **1998**, *205*, 205–212. [CrossRef] [PubMed]
24. Ge, S.; Shi, X.; Sun, K.; Li, C.; Uher, C.; Baker, J.R.; Holl, M.M.B.; Orr, B.G. Facile Hydrothermal Synthesis of Iron Oxide Nanoparticles with Tunable Magnetic Properties. *J. Phys. Chem. C* **2009**, *113*, 13593–13599. [CrossRef]
25. Daou, T.J.; Pourroy, G.; Begin-Colin, S.; Greneche, J.M.; Ulhaq-Bouillet, C.; Legare, P.; Bernhardt, P.; Leuvrey, C.; Rogez, G. Hydrothermal synthesis of monodisperse magnetite nanoparticles. *Chem. Mater.* **2006**, *18*, 4399–4404. [CrossRef]
26. Zhou, Z.H.; Wang, J.; Liu, X.; Chan, H.S.O. Synthesis of $Fe_3O_4$ nanoparticles from emulsions. *J. Mater. Chem.* **2001**, *11*, 1704–1709. [CrossRef]
27. Lee, Y.; Lee, J.; Bae, C.J.; Park, J.G.; Noh, H.J.; Park, J.H.; Hyeon, T. Large-scale synthesis of uniform and crystalline magnetite nanoparticles using reverse micelles as nanoreactors under reflux conditions. *Adv. Funct. Mater.* **2005**, *15*, 503–509. [CrossRef]
28. Hyeon, T.; Lee, S.S.; Park, J.; Chung, Y.; Bin Na, H. Synthesis of highly crystalline and monodisperse maghemite nanocrystallites without a size-selection process. *J. Am. Chem. Soc.* **2001**, *123*, 12798–12801. [CrossRef] [PubMed]
29. Pauly, M.; Pichon, B.P.; Albouy, P.-A.; Fleutot, S.; Leuvrey, C.; Trassin, M.; Gallani, J.-L.; Begin-Colin, S. Monolayer and multilayer assemblies of spherically and cubic-shaped iron oxide nanoparticles. *J. Mater. Chem.* **2011**, *21*, 16018–16027. [CrossRef]
30. Baaziz, W.; Pichon, B.P.; Fleutot, S.; Liu, Y.; Lefevre, C.; Greneche, J.-M.; Toumi, M.; Mhiri, T.; Begin-Colin, S. Magnetic Iron Oxide Nanoparticles: Reproducible Tuning of the Size and Nanosized-Dependent Composition, Defects, and Spin Canting. *J. Phys. Chem. C* **2014**, *118*, 3795–3810. [CrossRef]
31. Cai, W.; Wan, J. Facile synthesis of superparamagnetic magnetite nanoparticles in liquid polyols. *J. Colloid Interface Sci.* **2007**, *305*, 366–370. [CrossRef]
32. Arndt, D.; Zielasek, V.; Dreher, W.; Baeumer, M. Ethylene diamine-assisted synthesis of iron oxide nanoparticles in high-boiling polyolys. *J. Colloid Interface Sci.* **2014**, *417*, 188–198. [CrossRef]
33. Thomas, G.; Demoisson, F.; Boudon, J.; Millot, N. Efficient functionalization of magnetite nanoparticles with phosphonate using a one-step continuous hydrothermal process. *Dalton Trans.* **2016**, *45*, 10821–10829. [CrossRef]
34. Fouineau, J.; Brymora, K.; Ourry, L.; Mammeri, F.; Yaacoub, N.; Calvayrac, F.; Ammar-Merah, S.; Greneche, J.-M. Synthesis, Mössbauer Characterization, and Ab Initio Modeling of Iron Oxide Nanoparticles of Medical Interest Functionalized by Dopamine. *J. Phys. Chem. C* **2013**, *117*, 14295–14302. [CrossRef]
35. HongZhang, Q.; Biao, Y.; ChengKui, L.; Wei, L. Synthesis and characterization of water-soluble magnetite nanocrystals via one-step sol-gel pathway. *Sci. China Phys. Mech. Astron.* **2011**, *54*, 1239–1243.
36. Raja, K.; Jaculine, M.M.; Jose, M.; Verma, S.; Prince, A.A.M.; Ilangovan, K.; Sethusankar, K.; Das, S.J. Sol-gel synthesis and characterization of alpha-$Fe_2O_3$ nanoparticles. *Superlattices Microstruct.* **2015**, *86*, 306–312. [CrossRef]
37. Xu, Y.; Zhuang, L.; Lin, H.; Shen, H.; Li, J.W. Preparation and characterization of polyacrylic acid coated magnetite nanoparticles functionalized with amino acids. *Thin Solid Films* **2013**, *544*, 368–373. [CrossRef]
38. Sciancalepore, C.; Rosa, R.; Barrera, G.; Tiberto, P.; Allia, P.; Bondioli, F. Microwave-assisted nonaqueous sol-gel synthesis of highly crystalline magnetite nanocrystals. *Mater. Chem. Phys.* **2014**, *148*, 117–124. [CrossRef]
39. Ramos Guivar, J.A.; Sanches, E.A.; Bruns, F.; Sadrollahi, E.; Morales, M.A.; López, E.O.; Litterst, F.J. Vacancy ordered $\gamma$-$Fe_2O_3$ nanoparticles functionalized with nanohydroxyapatite: XRD, FTIR, TEM, XPS and Mössbauer studies. *Appl. Surf. Sci.* **2016**, *389*, 721–734. [CrossRef]
40. Saikia, C.; Das, M.K.; Ramteke, A.; Maji, T.K. Effect of crosslinker on drug delivery properties of curcumin loaded starch coated iron oxide nanoparticles. *Int. J. Biol. Macromol.* **2016**, *93*, 1121–1132. [CrossRef] [PubMed]
41. Mascolo, M.C.; Pei, Y.; Ring, T.A. Room Temperature Co-Precipitation Synthesis of Magnetite Nanoparticles in a Large pH Window with Different Bases. *Materials* **2013**, *6*, 5549–5567. [CrossRef] [PubMed]
42. El Ghandoor, H.; Zidan, H.M.; Khalil, M.M.H.; Ismail, M.I.M. Synthesis and Some Physical Properties of Magnetite ($Fe_3O_4$) Nanoparticles. *Int. J. Electrochem. Sci.* **2012**, *7*, 5734–5745.
43. Drbohlavova, J.; Hrdy, R.; Adam, V.; Kizek, R.; Schneeweiss, O.; Hubalek, J. Preparation and Properties of Various Magnetic Nanoparticles. *Sensors* **2009**, *9*, 2352–2362. [CrossRef]
44. Nath, S.; Kaittanis, C.; Ramachandran, V.; Dalal, N.S.; Perez, J.M. Synthesis, Magnetic Characterization, and Sensing Applications of Novel Dextran-Coated Iron Oxide Nanorods. *Chem. Mater.* **2009**, *21*, 1761–1767. [CrossRef]
45. Fazilati, M. Folate decorated magnetite nanoparticles: Synthesis and targeted therapy against ovarian cancer. *Cell Biol. Int.* **2014**, *38*, 154–163. [CrossRef]
46. Illes, E.; Szekeres, M.; Kupcsik, E.; Toth, I.Y.; Farkas, K.; Jedlovszky-Hajdu, A.; Tombacz, E. PEGylation of surfacted magnetite core-shell nanoparticles for biomedical application. *Colloids Surf. A Physicochem. Eng. Asp.* **2014**, *460*, 429–440. [CrossRef]
47. Maurizi, L.; Bisht, H.; Bouyer, F.; Millot, N. Easy route to functionalize iron oxide nanoparticles via long-term stable thiol groups. *Langmuir ACS J. Surf. Colloids* **2009**, *25*, 8857–8859. [CrossRef] [PubMed]
48. Milosevic, I.; Motte, L.; Aoun, B.; Li, T.; Ren, Y.; Sun, C.; Saboungi, M.-L. Effects of coating spherical iron oxide nanoparticles. *Biochim. Biophys. Acta BBA-Gen. Subj.* **2017**, *1861*, 3621–3626. [CrossRef] [PubMed]

49. Mazuel, F.; Espinosa, A.; Luciani, N.; Reffay, M.; Le Borgne, R.; Motte, L.; Desboeufs, K.; Michel, A.; Pellegrino, T.; Lalatonne, Y.; et al. Massive Intracellular Biodegradation of Iron Oxide Nanoparticles Evidenced Magnetically at Single-Endosome and Tissue Levels. *ACS Nano* **2016**, *10*, 7627–7638. [CrossRef]
50. Lamer, V.; Dinegar, R. Theory, Production and Mechanism of Formation of Monodispersed Hydrosols. *J. Am. Chem. Soc.* **1950**, *72*, 4847–4854. [CrossRef]
51. Baumgartner, J.; Dey, A.; Bomans, P.H.H.; Le Coadou, C.; Fratzl, P.; Sommerdijk, N.A.J.M.; Faivre, D. Nucleation and growth of magnetite from solution. *Nat. Mater.* **2013**, *12*, 310–314. [CrossRef] [PubMed]
52. Vreeland, E.C.; Watt, J.; Schober, G.B.; Hance, B.G.; Austin, M.J.; Price, A.D.; Fellows, B.D.; Monson, T.C.; Hudak, N.S.; Maldonado-Camargo, L.; et al. Enhanced Nanoparticle Size Control by Extending LaMer's Mechanism. *Chem. Mater.* **2015**, *27*, 6059–6066. [CrossRef]
53. Massart, R.; Dubois, E.; Cabuil, V.; Hasmonay, E. Preparation and Properties of Monodisperse Magnetic Fluids. *J. Magn. Magn. Mater.* **1995**, *149*, 1–5. [CrossRef]
54. Jolivet, J.; Belleville, P.; Tronc, E.; Livage, J. Influence of Fe(ii) on the Formation of the Spinel Iron-Oxide in Alkaline-Medium. *Clays Clay Miner.* **1992**, *40*, 531–539. [CrossRef]
55. Babes, L.; Denizot, B.; Tanguy, G.; Le Jeune, J.J.; Jallet, P. Synthesis of iron oxide nanoparticles used as MRI contrast agents: A parametric study. *J. Colloid Interface Sci.* **1999**, *212*, 474–482. [CrossRef]
56. Kim, D.K.; Zhang, Y.; Voit, W.; Rao, K.V.; Muhammed, M. Synthesis and characterization of surfactant-coated superparamagnetic monodispersed iron oxide nanoparticles. *J. Magn. Magn. Mater.* **2001**, *225*, 30–36. [CrossRef]
57. Liang, Y.-J.; Zhang, Y.; Guo, Z.; Xie, J.; Bai, T.; Zou, J.; Gu, N. Ultrafast Preparation of Monodisperse $Fe_3O_4$ Nanoparticles by Microwave-Assisted Thermal Decomposition. *Chem.—Eur. J.* **2016**, *22*, 11807–11815. [CrossRef] [PubMed]
58. Chikan, V.; McLaurin, E. Rapid Nanoparticle Synthesis by Magnetic and Microwave Heating. *Nanomaterials* **2016**, *6*, 85. [CrossRef] [PubMed]
59. Pascu, O.; Carenza, E.; Gich, M.; Estradé, S.; Peiro, F.; Herranz, G.; Roig, A. Surface Reactivity of Iron Oxide Nanoparticles by Microwave-Assisted Synthesis; Comparison with the Thermal Decomposition Route. *J. Phys. Chem. C* **2012**, *116*, 15108–15116. [CrossRef]
60. Wu, W.; Wu, Z.; Yu, T.; Jiang, C.; Kim, W.-S. Recent Progress on Magnetic Iron Oxide Nanoparticles: Synthesis, Surface Functional Strategies and Biomedical Applications. *Sci. Technol. Adv. Mater.* **2015**, *16*, 023501. [CrossRef] [PubMed]
61. Brollo, M.E.F.; Veintemillas-Verdaguer, S.; Salván, C.M.; del Puerto Morales, M. Key Parameters on the Microwave Assisted Synthesis of Magnetic Nanoparticles for MRI Contrast Agents. *Contrast Media Mol. Imaging* **2017**, *2017*, 8902424. [CrossRef]
62. Ai, Z.; Deng, K.; Wan, Q.; Zhang, L.; Lee, S. Facile Microwave-Assisted Synthesis and Magnetic and Gas Sensing Properties of Fe $_3$ O $_4$ Nanoroses. *J. Phys. Chem. C* **2010**, *114*, 6237–6242. [CrossRef]
63. Wu, L.; Yao, H.; Hu, B.; Yu, S.-H. Unique Lamellar Sodium/Potassium Iron Oxide Nanosheets: Facile Microwave-Assisted Synthesis and Magnetic and Electrochemical Properties. *Chem. Mater.* **2011**, *23*, 3946–3952. [CrossRef]
64. Hu, L.; Percheron, A.; Chaumont, D.; Brachais, C.-H. Microwave-Assisted One-Step Hydrothermal Synthesis of Pure Iron Oxide Nanoparticles: Magnetite, Maghemite and Hematite. *J. Sol-Gel Sci. Technol.* **2011**, *60*, 198–205. [CrossRef]
65. Liu, Z.; Miao, F.; Hua, W.; Zhao, F. Fe3O4 Nanoparticles: Microwave-Assisted Synthesis and Mechanism. *Mater. Lett.* **2012**, *67*, 358–361. [CrossRef]
66. Kowalczyk, B.; Lagzi, I.; Grzybowski, B.A. Nanoseparations: Strategies for size and/or shape-selective purification of nanoparticles. *Curr. Opin. Colloid Interface Sci.* **2011**, *16*, 135–148. [CrossRef]
67. Mori, Y. Size-Selective Separation Techniques for Nanoparticles in Liquid. *KONA Powder Part. J.* **2015**, *32*, 102–114. [CrossRef]
68. Robertson, J.D.; Rizzello, L.; Avila-Olias, M.; Gaitzsch, J.; Contini, C.; Magon, M.S.; Renshaw, S.A.; Battaglia, G. Purification of Nanoparticles by Size and Shape. *Sci. Rep.* **2016**, *6*, 27494. [CrossRef] [PubMed]
69. Costo, R.; Bello, V.; González-Carreño, T.; Veintemillas-Verdaguer, S.; Wang, D. Size sorting of ultrasmall magnetic nanoparticles and their aggregates behaviour. *Mater. Res. Bull.* **2013**, *48*, 4294–4300. [CrossRef]
70. Mireles, L.-K.; Sacher, E.; Yahia, L.; Laurent, S.; Stanicki, D. Washing effect on superparamagnetic iron oxide nanoparticles. *Data Brief* **2016**, *7*, 1296–1301. [CrossRef] [PubMed]
71. Lassenberger, A.; Bixner, O.; Gruenewald, T.; Lichtenegger, H.; Zirbs, R.; Reimhult, E. Evaluation of High-Yield Purification Methods on Monodisperse PEG-Grafted Iron Oxide Nanoparticles. *Langmuir* **2016**, *32*, 4259–4269. [CrossRef] [PubMed]
72. Qiu, P.; Mao, C. Viscosity Gradient as a Novel Mechanism for the Centrifugation-Based Separation of Nanoparticles. *Adv. Mater.* **2011**, *23*, 4880–4885. [CrossRef] [PubMed]
73. Bonaccorso, F.; Zerbetto, M.; Ferrari, A.C.; Amendola, V. Sorting Nanoparticles by Centrifugal Fields in Clean Media. *J. Phys. Chem. C* **2013**, *117*, 13217–13229. [CrossRef]
74. Akthakul, A.; Hochbaum, A.I.; Stellacci, F.; Mayes, A.M. Size Fractionation of Metal Nanoparticles by Membrane Filtration. *Adv. Mater.* **2005**, *17*, 532–535. [CrossRef]
75. Sweeney, S.F.; Woehrle, G.H.; Hutchison, J.E. Rapid Purification and Size Separation of Gold Nanoparticles via Diafiltration. *J. Am. Chem. Soc.* **2006**, *128*, 3190–3197. [CrossRef]
76. Snoswell, D.R.E.; Duan, J.; Fornasiero, D.; Ralston, J. The selective aggregation and separation of titania from a mixed suspension of silica and titania. *Int. J. Miner. Process.* **2005**, *78*, 1–10. [CrossRef]

77. Goloverda, G.; Jackson, B.; Kidd, C.; Kolesnichenko, V. Synthesis of ultrasmall magnetic iron oxide nanoparticles and study of their colloid and surface chemistry. *J. Magn. Magn. Mater.* **2009**, *321*, 1372–1376. [CrossRef] [PubMed]
78. Hollamby, M.J.; Eastoe, J.; Chemelli, A.; Glatter, O.; Rogers, S.; Heenan, R.K.; Grillo, I. Separation and Purification of Nanoparticles in a Single Step. *Langmuir* **2010**, *26*, 6989–6994. [CrossRef] [PubMed]
79. Shen, Y.; Weeranoppanant, N.; Xie, L.; Chen, Y.; Lusardi, M.R.; Imbrogno, J.; Bawendi, M.G.; Jensen, K.F. Multistage extraction platform for highly efficient and fully continuous purification of nanoparticles. *Nanoscale* **2017**, *9*, 7703–7707. [CrossRef] [PubMed]
80. Forge, D.; Gossuin, Y.; Roch, A.; Laurent, S.; Elst, L.V.; Muller, R.N. Development of magnetic chromatography to sort polydisperse nanoparticles in ferrofluids. *Contrast Media Mol. Imaging* **2010**, *5*, 126–132. [CrossRef]
81. Halverson, D.; Friedman, G. Magnetic Field Assisted Fractionation of Nonmagnetic Colloids in Ferrofluid. *IEEE Trans. Magn.* **2007**, *43*, 2692–2694. [CrossRef]
82. Ogrady, K.; Stewardson, H.; Chantrell, R.; Fletcher, D.; Unwin, D.; Parker, M. Magnetic Filtration of Ferrofluids. *IEEE Trans. Magn.* **1986**, *22*, 1134–1136. [CrossRef]
83. Bacri, J.; Perzynski, R.; Salin, D.; Cabuil, V.; Massart, R. Ionic Ferrofluids—A Crossing of Chemistry and Physics. *J. Magn. Magn. Mater.* **1990**, *85*, 27–32. [CrossRef]
84. Hola, K.; Markova, Z.; Zoppellaro, G.; Tucek, J.; Zboril, R. Tailored functionalization of iron oxide nanoparticles for MRI, drug delivery, magnetic separation and immobilization of biosubstances. *Biotechnol. Adv.* **2015**, *33*, 1162–1176. [CrossRef]
85. Berry, C.C.; Wells, S.; Charles, S.; Curtis, A.S.G. Dextran and albumin derivatised iron oxide nanoparticles: Influence on fibroblasts in vitro. *Biomaterials* **2003**, *24*, 4551–4557. [CrossRef]
86. Jiang, W.Q.; Yang, H.C.; Yang, S.Y.; Horng, H.E.; Hung, J.C.; Chen, Y.C.; Hong, C.Y. Preparation and properties of superparamagnetic nanoparticles with narrow size distribution and biocompatible. *J. Magn. Magn. Mater.* **2004**, *283*, 210–214. [CrossRef]
87. Shan, G.B.; Xing, J.M.; Luo, M.F.; Liu, H.Z.; Chen, J.Y. Immobilization of Pseudomonas delafieldii with magnetic polyvinyl alcohol beads and its application in biodesulfurization. *Biotechnol. Lett.* **2003**, *25*, 1977–1981. [CrossRef] [PubMed]
88. Mahmoudi, M.; Simchi, A.; Imani, M.; Milani, A.S.; Stroeve, P. Optimal Design and Characterization of Superparamagnetic Iron Oxide Nanoparticles Coated with Polyvinyl Alcohol for Targeted Delivery and Imaging. *J. Phys. Chem. B* **2008**, *112*, 14470–14481. [CrossRef] [PubMed]
89. Unsoy, G.; Yalcin, S.; Khodadust, R.; Gunduz, G.; Gunduz, U. Synthesis optimization and characterization of chitosan-coated iron oxide nanoparticles produced for biomedical applications. *J. Nanoparticle Res.* **2012**, *14*, 964. [CrossRef]
90. Lopez-Cruz, A.; Barrera, C.; Calero-DdelC, V.L.; Rinaldi, C. Water dispersible iron oxide nanoparticles coated with covalently linked chitosan. *J. Mater. Chem.* **2009**, *19*, 6870–6876. [CrossRef]
91. Bee, A.; Massart, R.; Neveu, S. Synthesis of Very Fine Maghemite Particles. *J. Magn. Magn. Mater.* **1995**, *149*, 6–9. [CrossRef]
92. Andreas, K.; Georgieva, R.; Ladwig, M.; Mueller, S.; Notter, M.; Sittinger, M.; Ringe, J. Highly efficient magnetic stem cell labeling with citrate-coated superparamagnetic iron oxide nanoparticles for MRI tracking. *Biomaterials* **2012**, *33*, 4515–4525. [CrossRef]
93. Sahoo, Y.; Pizem, H.; Fried, T.; Golodnitsky, D.; Burstein, L.; Sukenik, C.N.; Markovich, G. Alkyl phosphonate/phosphate coating on magnetite nanoparticles: A comparison with fatty acids. *Langmuir* **2001**, *17*, 7907–7911. [CrossRef]
94. Eskandari, H.; Shariati, M.R. Dodecylbenzene sulfonate-coated magnetite nanoparticles as a new adsorbent for solid phase extraction-spectrophotometric determination of ultra trace amounts of ammonium in water samples. *Anal. Chim. Acta* **2011**, *704*, 146–153. [CrossRef]
95. Xu, Z.; Hou, Y.; Sun, S. Magnetic core/shell $Fe_3O_4$/Au and $Fe_3O_4$/Au/Ag nanoparticles with tunable plasmonic properties. *J. Am. Chem. Soc.* **2007**, *129*, 8698–8699. [CrossRef]
96. Klotz, M.; Ayral, A.; Guizard, C.; Menager, C.; Cabuil, V. Silica coating on colloidal maghemite particles. *J. Colloid Interface Sci.* **1999**, *220*, 357–361. [CrossRef]
97. Liu, H.-M.; Wu, S.-H.; Lu, C.-W.; Yao, M.; Hsiao, J.-K.; Hung, Y.; Lin, Y.-S.; Mou, C.-Y.; Yang, C.-S.; Huang, D.-M.; et al. Mesoporous silica nanoparticles improve magnetic labeling efficiency in human stem cells. *Small* **2008**, *4*, 619–626. [CrossRef] [PubMed]
98. Gupta, A.K.; Wells, S. Surface-modified superparamagnetic nanoparticles for drug delivery: Preparation, characterization, and cytotoxicity studies. *IEEE Trans. Nanobiosci.* **2004**, *3*, 66–73. [CrossRef] [PubMed]
99. Zhang, Y.; Kohler, N.; Zhang, M.Q. Surface modification of superparamagnetic magnetite nanoparticles and their intracellular uptake. *Biomaterials* **2002**, *23*, 1553–1561. [CrossRef]
100. Schweiger, C.; Pietzonka, C.; Heverhagen, J.; Kissel, T. Novel magnetic iron oxide nanoparticles coated with poly(ethylene imine)-g-poly(ethylene glycol) for potential biomedical application: Synthesis, stability, cytotoxicity and MR imaging. *Int. J. Pharm.* **2011**, *408*, 130–137. [CrossRef] [PubMed]
101. Tombacz, E.; Bica, D.; Hajdu, A.; Illes, E.; Majzik, A.; Vekas, L. Surfactant double layer stabilized magnetic nanofluids for biomedical application. *J. Phys.-Condens. Matter* **2008**, *20*, 204103. [CrossRef]
102. Maurizi, L.; Bouyer, F.; Paris, J.; Demoisson, F.; Saviot, L.; Millot, N. One step continuous hydrothermal synthesis of very fine stabilized superparamagnetic nanoparticles of magnetite. *Chem. Commun. Camb. Engl.* **2011**, *47*, 11706–11708. [CrossRef]
103. Bart, A.; Heldreth, M.M.F. Final Report: On the Safety Assessment of Citric Acid, Innorganic Citrate Salts, and Alkyl Citrate Esters as Used in Cosmetics. 2012. Available online: http://www.cir-safety.org/sites/default/files/citric032012FR.pdf (accessed on 15 July 2022).
104. Cheng, C.-M.; Kou, G.; Wang, X.-L.; Wang, S.-H.; Gu, H.-C.; Guo, Y.-J. Synthesis of carboxyl superparamagnetic ultrasmall iron oxide (USPIO) nanoparticles by a novel flocculation-redispersion process. *J. Magn. Magn. Mater.* **2009**, *321*, 2663–2669. [CrossRef]

105. Bishop, L.M.; Yeager, J.C.; Chen, X.; Wheeler, J.N.; Torelli, M.D.; Benson, M.C.; Burke, S.D.; Pedersen, J.A.; Hamers, R.J. A Citric Acid-Derived Ligand for Modular Functionalization of Metal Oxide Surfaces via 'Click' Chemistry. *Langmuir* **2012**, *28*, 1322–1329. [CrossRef]
106. Huisgen, R. Kinetics and Mechanism of 1,3-Dipolar Cycloadditions. *Angew. Chem. Int. Ed. Engl.* **1963**, *2*, 633–645. [CrossRef]